J Mater Sci: Mater Electron (2016) 27:3845–3853
DOI 10.1007/s10854-015-4232-4

Impedance, scaling behavior and conduction mechanism in double perovskite Pr_2CuZrO_6 ceramic

Dev K. Mahato[1] · Sujoy Saha[2] · T. P. Sinha[2]

Received: 24 October 2015 / Accepted: 14 December 2015 / Published online: 20 January 2016

Abstract Double perovskite oxide Pr_2CuZrO_6 (PCZO) has been synthesized by solid-state reaction technique in the temperature range from 30 to 310 °C and in the temperature range from 100 Hz to 1 MHz. The X-ray diffraction pattern of the sample at room temperature shows monoclinic structure. An analysis of the real and imaginary parts of impedance as well as electric modulus shows a distribution of relaxation times. The Cole–Cole model is used to investigate the relaxation mechanism of PCZO. The frequency-dependent maxima in the imaginary impedance and imaginary electric modulus are found to obey an Arrhenius law with activation energy ~0.35 eV. The frequency-dependent electrical data is also analyzed in the framework of conductivity. The combined Z''/Z''_m and M''/M''_m plots indicates that the charge carriers are localized in PCZO in the higher temperature range. The ac conductivity spectra follow the universal power law and Summerfield scaling.

1 Introduction

Electroceramics are high technology materials whose properties and applications depend on the close control of structure, composition, ceramic texture, dopants and defect distribution. With the rapid development of microelectronic devices such as capacitors, resonators and filters, electroceramics belonging to ABO_3 perovskite family have been on an increasing demand. The ABO_3 perovskites can be extended by substitutions at the A and B-site cations to optimize their physical properties for specific applications. When the octahedrally coordinated B cations are occupied by two kinds of B′ and B″ cations with large difference in charge and/or size, it forms double perovskite oxide (DPO) of general formula $A_2B'B''O_6$. In $A_2B'B''O_6$, the A site is occupied by alkaline earth metals or rare earth ions of larger ionic radii, B′ and B″ octahedral sites are occupied by the transition metal cations or lanthanides with smaller ionic radii [1]. Although oxides of the type $A_2B'B''O_6$ have known since long ago [2–5], they are receiving a renewed great deal of attention due to their unique dielectric, electrical and magnetic properties. Recently a large number of new DPOs have been investigated for their dielectric. Due to the complicated characteristics and interesting combination of various properties (e.g. at high frequencies (viz. >100 kHz) the dielectric properties of DPOs due to grain interior), DPOs have become very exciting materials for investigators. The electrical properties of double perovskite Pr_2CuZrO_6 with rare earth ions Pr^{3+} at A-site and non-magnetic elements such as Cu and Zr at B-site have not been extensively investigated and reported to the best of our knowledge. This has motivated us to investigate the electrical properties of Pr_2CuZrO_6 at high frequencies (>100 kHz) to establish the domination of the grains to the electrical properties of the material.

In the present work, Pr_2CuZrO_6 ceramic are prepared by solid-state sintering process, and electrical properties are investigated in a broad frequency (100 Hz–1 MHz) and temperature range (30–310 °C).

2 Experimental procedure

Polycrystalline sample of Pr_2CuZrO_6 (PCZO) is prepared by conventional solid-state reaction route using high purity powders of Pr_2O_3 (Aldrich 99.9 %), CuO (Loba Chemie

✉ Dev K. Mahato
drdevkumar@yahoo.com

[1] Department of Physics, National Institute of Technology Patna, Patna 800 005, India

[2] Department of Physics, Bose Institute, 93/1, Acharya Prafulla Chandra Road, Kolkata 700009, India

99 %) and ZrO_2 (Loba Chemie 99.5 %) as ingredient. These ingredients, taken in stoichiometric ratio, are thoroughly mixed in an agate mortar in the presence of acetone (MERCK) for 12 h. The mixture is calcined in a Pt crucible at 1100 °C in air for 10 h and brought to room temperature at a cooling rate of 100 °C/h. The calcined sample is palletized into a circular disc (of thickness 2 mm and diameter 8 mm) using PVA as a binder. The palletized discs are sintered at 1150 °C for 5 h and then cooled down to room temperature by adjusting the cooling rate. The determination of lattice parameters and the identification of the phases are carried out using an X-ray powder diffractometer (Rigaku Miniflex-II). The X-ray diffraction (XRD) patterns of the sample is collected in a wide range of Bragg angles ($20° \leq 2\theta \leq 80°$) using CuK_α radiation ($\lambda = 1.5418$ Å) and a Ni filter operating at 30 kV and 15 mA at a scanning rate of 2° min^{-1}. Scanning electron micrographs of the sample is taken by FEI QUANTA 200 scanning electron microscope.

For the electrical measurements, the pellets are polished to make both of their faces flat and parallel and electroded by high purity ultrafine silver paste. To overcome the effect of moisture, if any, on electric properties the pellets are heated at 200 °C for 2 h and then cooled to room temperature prior to conducting experiment. Capacitance (C), impedance (Z), phase angle (φ) and conductance (G), of the sample are measured in the frequency range 100 Hz–1 MHz at various temperatures (30–310 °C) using a computer controlled LCR-meter (HIOKI-3532-50, Japan) with heating rate of 0.5 °C/min. The temperature is controlled by Eurotherm 818 P programmable temperature controller connected with the oven. Each measured temperature is kept constant with an accuracy ±1 °C.

3 Results and discussion

3.1 Structural characterization

The X-ray diffraction pattern of PCZO measured at room temperature is shown in Fig. 1. In this pattern sharp diffraction peaks are observed which are different from those of ingredients. This confirms the formation of single-phase compound. All the diffraction peaks of the X-ray profile are indexed taking their 2θ values and lattice parameters are determined using a least-squares refinement with the help of a standard computer programme Crysfire. On the basis of good agreement between the observed and calculated interplanar spacing d-values (i.e. $\Sigma(d_{obs}-d_{cal}) = \text{minimum}$), a monoclinic phase at room temperature is confirmed with a = 6.927 (2) Å, b = 6.563 (1) c = 6.168 (2) Å, β = 90.63° (3) and cell volume = 280.42 $Å^3$. SEM is capable of examining a relatively large field of view, thus providing detailed information on grain growth, porosity and its uniformity, as well as the regularity of pattern arrays. The SEM image shown in the inset of Fig. 1 indicates that the sample has a uniform distribution of grains with average particle size of 0.550 ± 0.002 μm. From the SEM image we observe the compactness of the sample is good. There is hardly any visible porosity in the sample and hence the electrical properties of the material should be due to grain interior only.

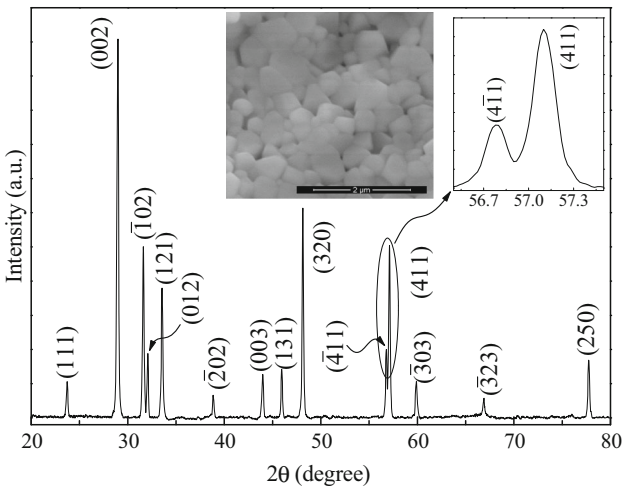

Fig. 1 XRD diffraction pattern of Pr_2CuZrO_6 at room temperature. SEM image of the sample is shown in the *inset*

3.2 Impedance study

Figure 2 shows the angular frequency dependence of the real part, Z′(ω) of impedance of PCZO at various temperatures. The variation of Z′ with frequency for all temperatures implies relaxation process in the sample. The Z′ values merge at higher frequencies for all temperatures indicating release of space charges as a result of reduction in the barrier properties (i.e. reduction of grains, grains boundaries and electrode interface resistance) of the material. Further, at low frequencies the value of Z′ decreases with rise in temperature showing negative temperature coefficient of resistance type behaviour.

Figure 3 shows the variation of the imaginary part Z″ (ω) of impedance of PCZO as a function of temperature. In Fig. 3 the curves show that the Z″ reaches a maximum value (Z''_m) and the value of Z''_m shifts to higher frequencies with increasing temperature. The decrease in impedance with an increase of temperature across the entire frequency range indicates the semiconducting behavior of the material. A typical peak broadening, which is slightly asymmetrical in nature, can be observed with the rise in temperature. The width of the peak in Fig. 3 points

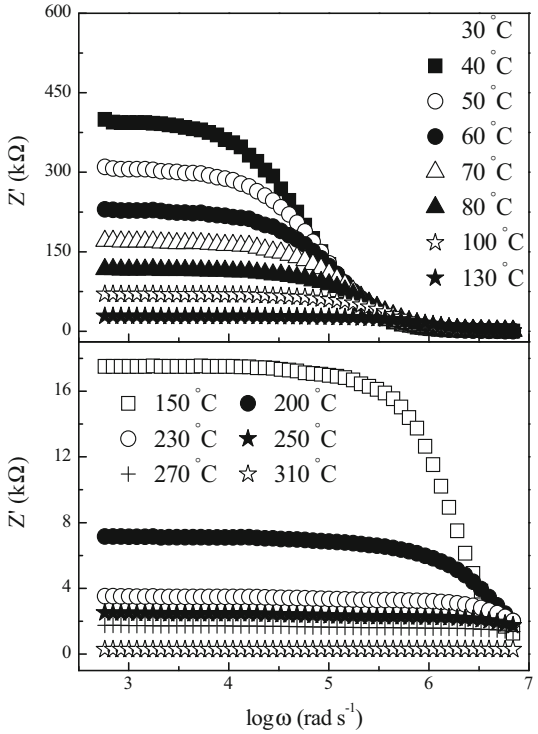

Fig. 2 Angular frequency dependence of the real part (Z′) of impedance of Pr_2CuZrO_6 at various temperatures

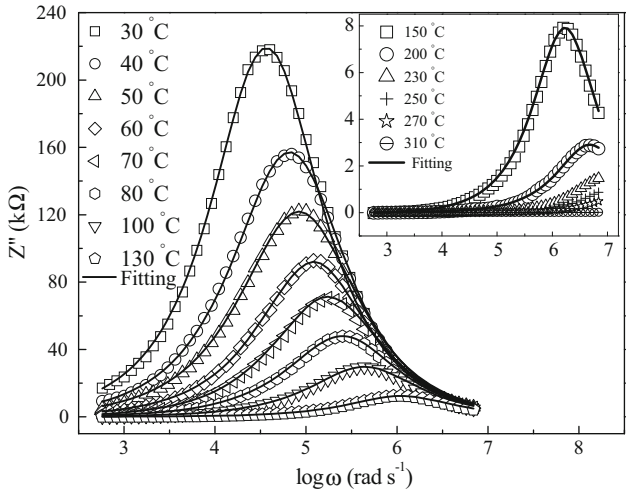

Fig. 3 Angular frequency dependence of the imaginary part (Z″) of impedance of Pr_2CuZrO_6 at various temperatures. The *solid lines* are fits of the impedance curves to Eq. (1)

towards the possibility of a distribution of relaxation times (i.e. the polydispersive nature of the material). One of the most convenient ways of checking the polydispersive nature of the material is to use Cole–Cole relation defined as [6].

$$Z^* = R_\infty + (R_0 - R_\infty)/[1 + (j\omega\tau_c)^\alpha] \quad (1)$$

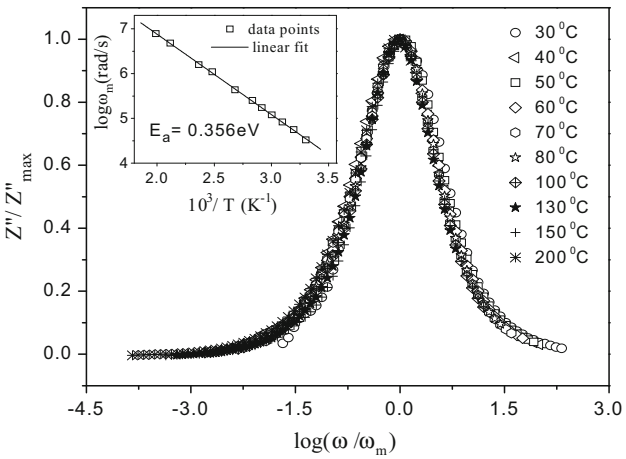

Fig. 4 Scaling behaviour of Z″ at various temperatures of Pr_2CuZrO_6. The temperature dependence of the most probable relaxation frequency is shown in the *inset* where the *symbols* are the experimental points and the *solid line* is the least-squares straight line fit

where R_0 and R_∞ are the resistances at very low and very high frequencies respectively and τ_c is the characteristic relaxation time of the system corresponding to the characteristic angular frequency ω at the peak position of Z″ in the Z″ versus log ω plot. α is the dimensionless exponent that denotes the angle of tilt of the circular arc from the real axis. The best fitting of the impedance data with Eq. (1) is shown by solid lines in Fig. 3. The value of α lie in the range of 0.71–0.72 in the temperature range of 30–200 °C.

A plot of the log ω_m versus of absolute temperature (1/T) is shown in the inset of Fig. 4, where the circles are the experimental data and the solid line is the least-square straight-line fit. The activation energy E_a calculated from the least-square fit to the points is found to be 0.356 eV. If we plot the Z″(ω,T) data in the scaled coordinates i.e. $Z''(\omega,T)/Z''_m$ and log (ω/ω_m), where ω_m corresponds to the frequency of the peak value of Z″ in the Z″ versus logω plots, the entire data of imaginary part of impedance can collapse into a single master curve as shown in Fig. 4. Thus the scaling confirms that the relaxation shape is temperature independent but the Arrhenius law is still operative meaning that the relaxation time is exponentially temperature dependent. The fact that the relaxation stays singly dispersed on the whole temperature range is quite expected when the relaxation process results from long range motion of free charges.

Figure 5 shows a set of impedance data taken over a wide frequency range (100 Hz–1 MHz) at several temperatures as a Nyquist plot (complex impedance plot) for PCZO. In the impedance spectrum, only single semicircular arcs (hollow curves) are observed at all temperatures with nonzero intercept at high frequencies (not shown here)

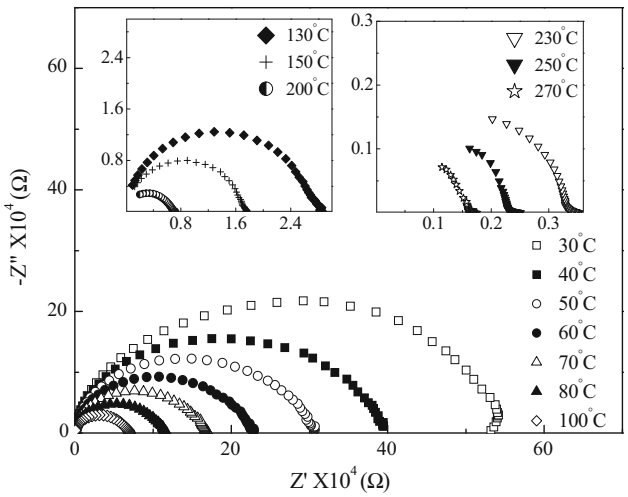

Fig. 5 Complex-plane impedance plots for Pr_2CuZrO_6 at various temperatures

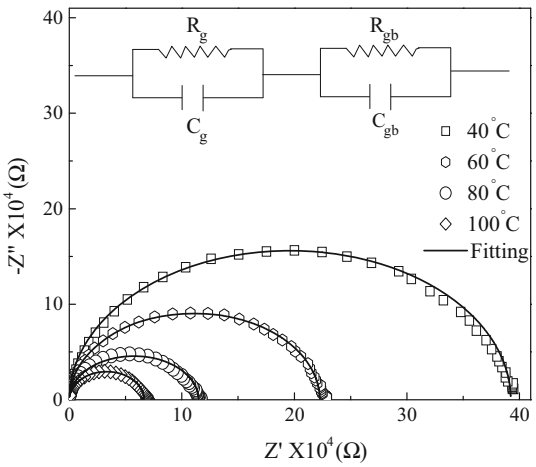

Fig. 6 Complex impedance spectrum of Pr_2CuZrO_6 at 40, 60 80 and 100 °C temperatures. *Solid line* is the fitting to the experimental data by RC equivalent circuit

which indicate that the sample is electrical inhomogeneous. The nonzero intercept indicates the presence of an arc for frequency higher than the maximum frequency measured (1 MHz), which is assigned as the contribution from grain interior while the large semicircular arc at low frequencies originates from the grain boundaries [7, 8]. In any material the grain, grain boundary and electrode effect may be seen in the experimental frequency window [9]. Due to the compactness or porosity of the sample we can observe only few. Regardless of the grain size there should be electrode effect whatever small, in the low frequency region (<50 Hz) above ~200 °C. The grain and grain boundary effect depends on the grain size as well the temperature. In general if the grains are large (~1 μm) we should get a visible grain/bulk effect below 1 MHz [10]. In the nanoceramics which have the grain size below 100 nm does not show any grain effect in a frequency below 1 MHz [11]. It is observed that the centre of the semicircular arc shifts towards the origin on increasing temperature which indicates that the conductivity of the samples increases with the increase in temperature. Figure 6 presents a typical complex impedance plane plot of PCZO compound and the corresponding equivalent circuit (inset of Fig. 6) at 40, 60, 80 and 100 °C. The values of grain and grain-boundary resistances and capacitances can be obtained by an equivalent circuit of two parallel resistance–capacitance (RC) elements connected in series. The equivalent electrical equations for grain and grain boundary are

$$Z' = R_s + \frac{R_g}{1 + (\omega R_g C_g)^2} + \frac{R_{gb}}{1 + (\omega R_{gb} C_{gb})^2} \quad (2)$$

Table1 As obtained from the intercept of the low frequency semicircle with the x-axis the values of R_{gb} and R_g and corresponding C_{gb} values

Temp (°C)	R_{gb} (Ω)	C_{gb} (F)	R_g (Ω)
40	391,877.55	4.420×10^{-11}	400.12
60	226,653.06	3.658×10^{-11}	445.97
80	114,326.53	3.471×10^{-11}	535.24
100	73,183.67	3.120×10^{-11}	667.62

and

$$Z'' = R_g \left[\frac{\omega R_g C_g}{1 + (\omega R_g C_g)^2} \right] + R_{gb} \left[\frac{\omega R_{gb} C_{gb}}{1 + (\omega R_{gb} C_{gb})^2} \right] \quad (3)$$

where, C_g and C_{gb} are the grain and grain-boundary capacitances and R_g and R_{gb} are the grain and grain–boundary resistances. We have fitted our experimental data with Eqs. (2) and (3) as shown by solid lines in Fig. 6. The values of the fitted parameters R_g, R_{gb}, and C_{gb} are given in Table 1.

3.3 Modulus formalism

Figure 7 shows the variation of real M′(ω) and imaginary M″(ω) parts of the complex electric modulus (M^*) as a function of frequency of PCZO at various temperatures. The real part of electric modulus (M′) in Fig. 7a shows a dispersion tending towards M_∞ (high frequency asymptotic value of M′) i.e. at high frequencies, M′(ω) approaches a maximum M_∞ and at low frequencies M′

approaches to zero which indicates that the electrode polarization makes a negligible or low contribution to M′. The value of M′ increases from low frequency towards a high frequency limit and the dispersion shifts to high frequency as temperature increases. The dispersion in between low and high frequencies is due to the conductivity relaxation. At higher temperatures and at higher frequencies, M_∞ levels off because the relaxation processes are spread over a range of frequencies. The peaks developed in the values of imaginary parts of electric modulus M″(ω) indicate a relaxation process Fig. 7b. The peak position shifts towards higher frequency side with an increase of temperature indicating the thermally activated nature of the relaxation time. For temperatures higher than 200 °C, the peaks are not observed and are probably beyond the range of experimental frequency window. Two apparent relaxation regions appear towards left of the peak associated with the conduction process where the charge carriers are mobile over a long distance; the region towards right of the peak associated with the relaxation polarization process where the charge carriers are spatially confined to the potential wells. Further, the height of the modulus peak appears to increase with rise in temperature suggesting a corresponding decrease in the capacitance value with temperature. In a relaxation process, one can determine the most probable relaxation time τ_m (= $1/\omega_m$) from the position of the peak in the M″ versus logω plot. The most probable relaxation time obeys the Arrhenius law

$$\tau_m = \tau_0 \exp\left(\frac{E_a}{k_B T}\right) \quad (4)$$

Where τ_0 is the pre-exponential factor, E_a is the activation energy, k_B is Boltzmann constant and T is the absolute temperature. A plot of the $\log\omega_m$ versus $10^3/T$ obtained from the frequency dependent plots of M″ for PCZO is shown in the inset of Fig. 8, where the symbols are the experimental data and the solid lines are the least squares straight-line fit. The activation energy of the compound calculated from the slope of $\log\omega_m$ versus $10^3/T$ is found to be 0.320 eV, which may be interpreted as polaron hopping based on electron carrier.

The scaling behavior of M″ i.e. M''/M''_m versus log (ω/ω_m) plot of PCZO at various temperatures is shown in Fig. 8, where M''_m represents the peak value of imaginary parts of electric modulus and ω_m corresponds to the frequency of the peak position of M″ in the M″ versus logω plots. The overlapping of the curves for all the temperatures into a single master curve indicates that the relaxation in PCZO describe the same mechanism at various temperatures. In other words, the coincidence of all the curves at different temperatures into a single master curve indicates temperature independence of dynamic processes.

The variation of normalized parameters Z''/Z''_m and M''/M''_m as a function of logarithmic frequency measured at 30–70 °C is plotted in Fig. 9 and 80–150 °C in Fig. 10 for PCZO. Comparison with the impedance and electrical modulus data determine the bulk response in terms of localized (defect relaxation) or non-localized conduction (ionic or electronic conductivity) [13]. The combined Z''/Z''_m and M''/M''_m plots is used to scale the extent of charge carriers been localized [14]. The overlapping of peak

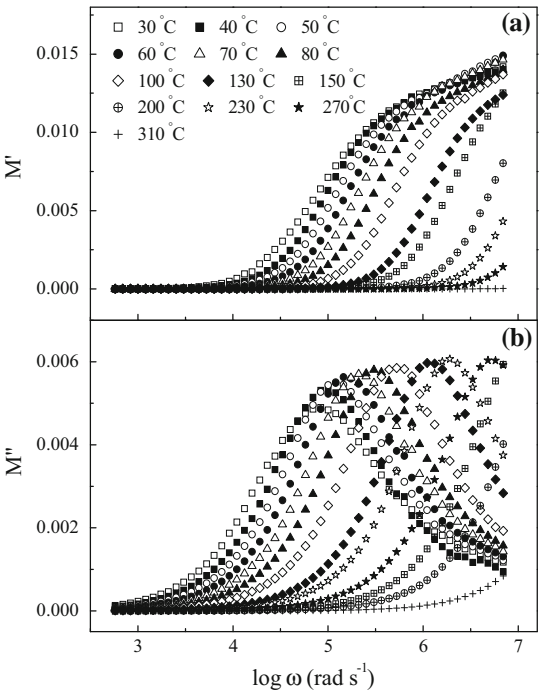

Fig. 7 Frequency dependence of **a** M′ and **b** M″ of Pr_2CuZrO_6 at various temperatures

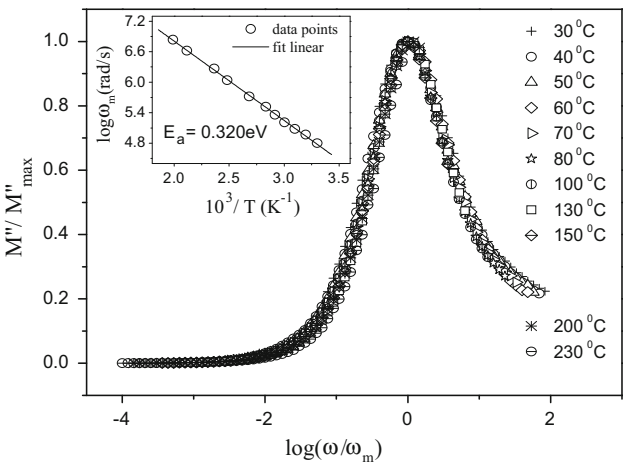

Fig. 8 Scaling behaviour of M″ at various temperatures for Pr_2CuZrO_6. *Inset* the temperature dependence of the most probable relaxation frequency obtained from the frequency-dependent plot of M″, where the *symbols* are the experimental points and the *solid line* is the least-squares straight line fit

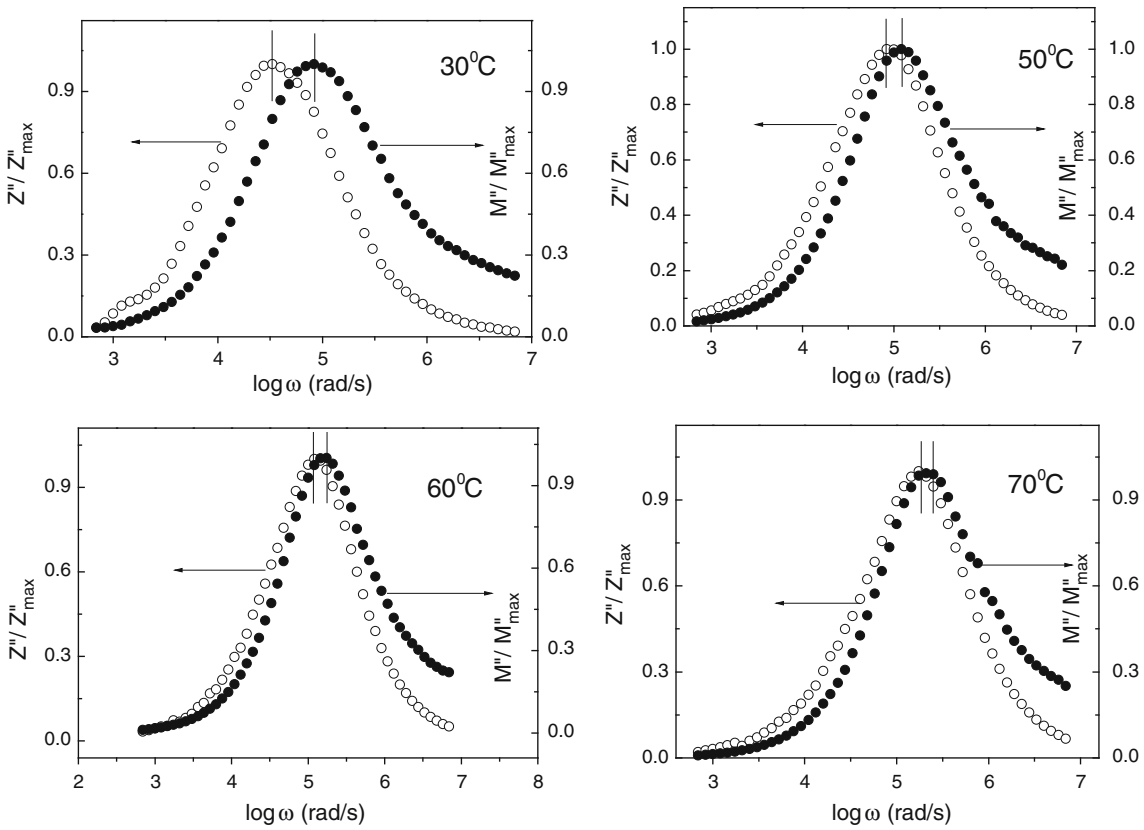

Fig. 9 Frequency dependence of normalized peaks Z''/Z''_m and M''/M''_m for Pr_2CuZrO_6 at various temperatures (30–70 °C)

positions between Z''/Z''_m and M''/M''_m curves suggests delocalized or long range relaxation of charge carriers [13]. On the other hand, if separation occurred, it indicates that the charge carriers are locally refined and can only make short range movement in terms of hopping. From Fig. 9 of the combined spectroscopy of impedance and electrical modulus, obvious separation of the peak frequencies between Z''/Z''_m and M''/M''_m is observed which decreases with increase in temperatures 30–70 °C. In Fig. 10 the peak separation goes on dectrasing with increase in temperature and finally the perfect coincidence of peaks between Z''/Z''_m and M''/M''_m occur at 150 °C. Therefore, it is proposed that in PCZO, short-range movement of the charge carriers is dominant at lower temperatures corresponds to localized relaxation and long range electronic conduction is dominant at higher temperatures. Figures 9 and 10 show the Z''/Z''_m and M''/M''_m do not overlap but are very close in the temperature range 70–130 °C, suggesting the presence of both long-range and localized relaxation.

3.4 AC conductivity study

The frequency dependence of ac conductivity (σ_{ac}) for PCZO at various temperatures is shown in Fig. 11. It is observed that at low frequencies and high temperatures plateaus of σ_{ac} appear (i.e. conductivity does not depends on frequency) which corresponds to the dc conductivity (σ_{dc}). The value of σ_{dc} is found to increase with an increase of temperature showing the semiconducting behavior of the material. The conductivity spectra follow the Jonscher power law [15] defined as:

$$\sigma = \sigma_{dc}\left[1 + \left(\frac{\omega}{\omega_H}\right)^n\right] \quad (5)$$

where, ω_H is the hopping frequency of charge carriers, and n is the dimensionless frequency exponent. The experimental conductivity data of PCZO are fitted to Eq. (5) with σ_{dc} and ω_H as variables keeping in mind that the values of parameter n are weakly temperature dependent. The best fit of conductivity spectra is shown by solid lines in Fig. 11 at various temperatures (30–270 °C). The reciprocal temperature dependence of σ_{dc} is shown in the inset of Fig. 12 which follows Arrhenius law with an activation energy of 0.357 eV. The activation energies of the compound calculated from impedance (0.356 eV), modulus spectrum (0.320 eV) and conductivity (0.357 eV) are the same and hence the relaxation mechanism may be attributed to the same type of charge carrier. Such a value of activation

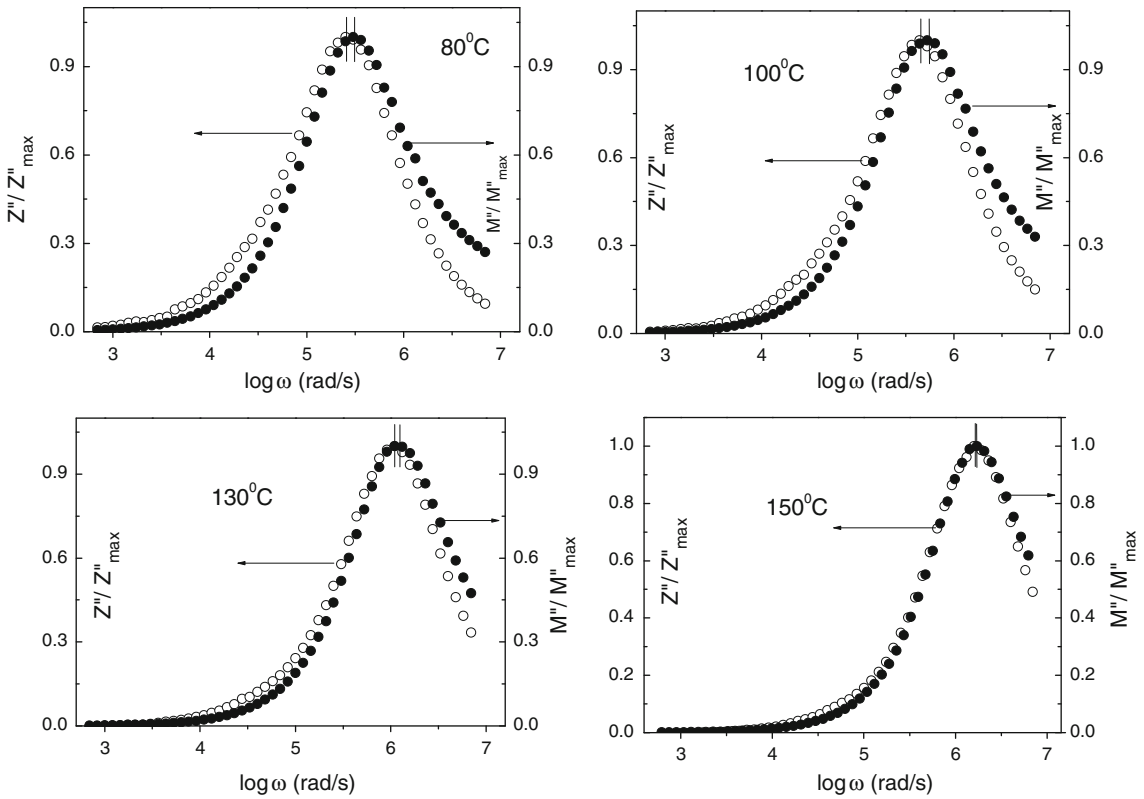

Fig. 10 Frequency dependence of normalized peaks Z''/Z''_m and M''/M''_m for Pr_2CuZrO_6 at various temperatures (80–150 °C)

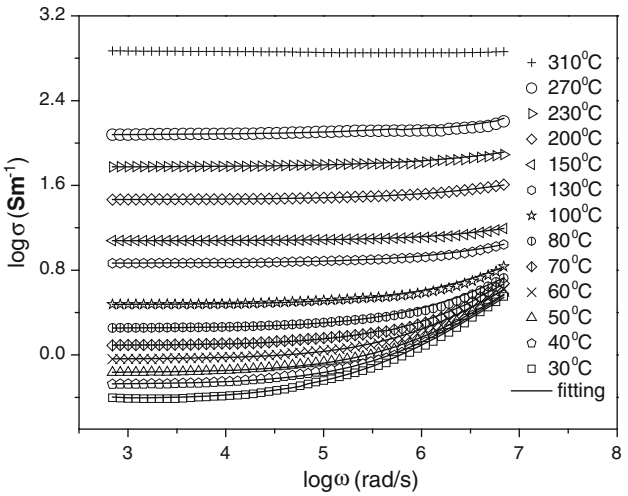

Fig. 11 Frequency dependence ac conductivity (σ_{ac}) of Pr_2CuZrO_6 at various temperatures where the *symbols* are the experimental points and the *solid lines* represent the fitting to Eq. (5)

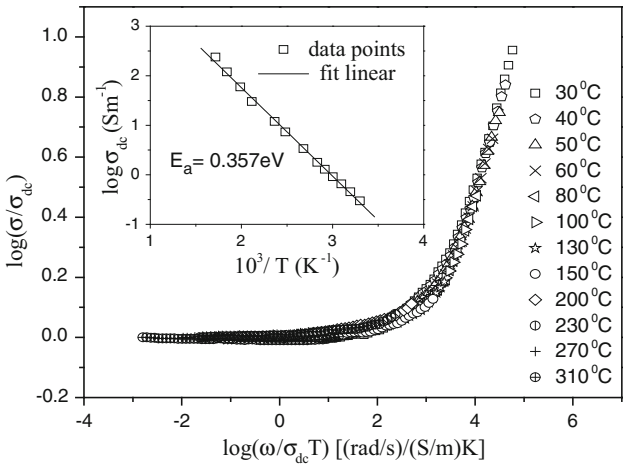

Fig. 12 Summerfield scaling for conductivity spectra at different temperatures of Pr_2CuZrO_6. *Inset* the temperature dependence of dc conductivity curve for Pr_2CuZrO_6, where the *symbols* are the experimental points and the *solid line* is the least-squares straight line fit

energy suggests that the conduction mechanism in PCZO may be due to the hopping of small polaron between neighboring sites within the crystal lattice and are consistent with our earlier reports [16, 17]. In highly polarizable lattices like perovskite oxides electronic localization results in a lattice deformation and polarization. Since such polarons are carrying a charge, an electronic dipole moment and an elastic energy.

In our earlier work [18] we have reported the activation energy of Ho_2CuZrO_6 (HCZ) as $\sim$0.1 eV. This indicates that the replacement of the Ho (A-site) by Pr ion leads to a

major role in the conduction mechanism. The conductivity of PCZO is higher than that of the HCZ. This is due to the decrease of ionic radius from Pr to Ho. A decrease in the ionic radius will increase the distortion in the material creating less hybridization between B′–O/B″–O which lowers the conductivity.

Figure 12 shows $\log(\sigma_{ac}/\sigma_{dc})$ versus $\log(\omega/\sigma_{dc}T)$ plot at different temperatures for PCZO. This so-called Summerfield scaling [19, 20] uses the directly measurable quantities σ_{dc} and T as the scaling parameter. From Fig. 12, it is obviously seen that a quite satisfying overlap of the data at different temperatures on a single master curve illustrates well the dynamic processes occurring at different frequencies need almost the same thermal activation energy. Another indication of those scaled master curves is that all Arrhenius temperature dependence of conductivity is embedded in the dc conductivity term.

Figure 13 illustrates the reciprocal temperature dependence of ac conductivity (σ_{ac}). It is observed that ac conductivity increases with rise in temperature and frequency. The increase of conductivity with temperature once again supports the negative temperature coefficient of resistance (NTCR) behaviour in the sample. The increase of σ_{ac} with rise in frequency may be attributed to the disordering of cations between neighbouring sites, and presence of space charges [21]. Ac conductivity activation energy decreases with increasing frequency from 0.343 to 0.224 eV and different activation energies involved in different temperature regions in the conduction process. The temperature dependence of hopping frequency is shown in the inset of Fig. 13. The hopping frequency ω_H increases with increase in temperature corresponds to short range to long range motion of charge carriers as discussed in Sect. 3.3. The hopping frequency ω_H also follows the Arrhenius law with the value of activation energy being 0.332 eV corresponds to that calculated from impedance, modulus and conductivity plots and once again confirms the polaron hopping.

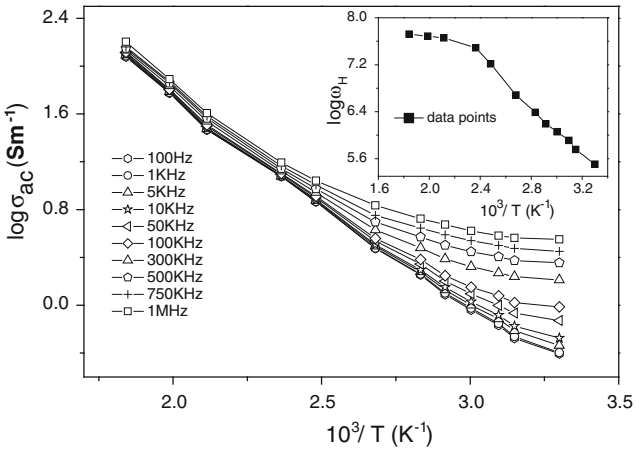

Fig. 13 Reciprocal temperature dependence of ac conductivity for Pr_2CuZrO_6 at different frequencies. *Inset* the temperature dependence of hopping frequency (ω_H)

4 Conclusions

The polycrystalline sample of Pr_2CuZrO_6 was prepared by solid-state sintering process, and electrical properties were investigated in a broad frequency (100 Hz–1 MHz) and temperature range (30–310 °C). The X-ray diffraction studies confirm the monoclinic crystal structure at room temperature with lattice parameters a = 6.927 (2) Å, b = 6.563 (1) c = 6.168 (2) Å, β = 90.63° (3). Based on an analysis of the impedance spectra, it has been shown that the nonzero intercept in impedance plane plot indicates the presence of grain boundary effect. The variation of dc conductivity as a function of temperature demonstrate that the compound exhibit Arrhenius type of electrical conductivity and semiconducting behaviour. Activation energies show that the conduction mechanism in PCZO may be due to the polaron hopping. From modulus study it has been observed that the dispersion in between low and high frequencies is due to the conductivity relaxation. The peak position shifts towards higher frequency side with an increase of temperature indicating the thermally activated nature of the relaxation time. The combined Z''/Z''_m and M''/M''_m plots confirmed that the presence of both long-range and localized relaxation of charge carriers were present in PCZO in the temperature range 70–130 °C.

Acknowledgments Sujoy Saha acknowledges the financial support provided by the UGC New Delhi in the form of SRF.

References

1. D. Iwanaga, Y. Inaguma, M. Itoh, J. Solid State Chem. **147**, 291 (1999)
2. F. Patterson, C. Moeller, R. Ward, Inorg. Chem. **2**, 196 (1963)
3. F. Galasso, F.C. Douglas, R.J. Kasper, J. Chem. Phys. **44**, 1672 (1966)
4. T. Nakagawa, J. Phys. Soc. Jap. **24**, 806 (1968)
5. M. Ito, I. Ohta, Y. Inaguma, Mater. Sci. Eng. B **41**, 55 (1996)
6. K.S. Cole, Cold Spring Harb. Symp. Quant. Biol. **8**, 110 (1940)
7. T.B. Adams, D.C. Sinclair, A.R. West, Adv. Mater. **14**, 1321 (2002)
8. D.C. Sinclair, T.B. Adams, F.D. Morrison, A.R. West, Appl. Phys. Lett. **80**, 2153 (2002)
9. R.K. Dwivedi, D. Kumar, O. Parkash, J. Mat. Sci. **36**, 3657 (2001)
10. S. Saha, S. Chanda, A. Dutta, T.P. Sinha, J. Sol-Gel Sci. Tech. **69**, 553 (2014)
11. A. Dutta, T.P. Sinha, Mat. Res. Bull. **46**, 518 (2011)
12. R.N.P. Choudhary, D.K. Pradhan, C.M. Tirado, G.E. Bonilla, R.S. Katiyar, Phys. Status Solidi (b) **244**, 2254 (2007)
13. R. Gerhardt, J. Phys. Chem. Solids **55**, 1491 (1994)

14. Q.Q. Ke, X.J. Lou, Y. Wang, J. Wang, Phys. Rev. B **82**, 024102 (2010)
15. A.K. Jonscher, *Dielectric Relaxation in Solids* (Chelsea Dielectric Press, London, 1983)
16. D.K. Mahato, A. Dutta, T.P. Sinha, Mat. Res. Bull **47**, 4226 (2012)
17. A. Dutta, T.P. Sinha, Mat. Res. Bull. **46**, 518 (2011)
18. D.K. Mahato, A. Dutta, N. Kumar, T.P. Sinha, Phys. Scr. **84**, 015602 (2011)
19. S. Summerfield, Philos. Mag. B **52**, 9 (1985)
20. N. Balkan, P.N. Batcher, W.R. Hogg, A.R. Long, S. Summerfield, Philos. B. Mag **51**, 7 (1985)
21. R. Padhee, P.R. Das, B.N. Parida, R.N.P. Choudhary, J. Mater. Sci.: Mater. Electron. **24**, 799 (2013)